American Mineralogist, Volume 97, pages 1515–1518, 2012

LETTER

Gold-telluride nanoparticles revealed in arsenic-free pyrite

CRISTIANA L. CIOBANU,[1,*] NIGEL J. COOK,[1] SATOSHI UTSUNOMIYA,[2] MASASHI KOGAGWA,[2] LEONARD GREEN,[3] SARAH GILBERT,[4] AND BENJAMIN WADE[3]

[1]Centre for Tectonics, Resources, and Exploration (TRaX), School of Earth and Environmental Sciences, University of Adelaide, 5005 South Australia, Australia
[2]Department of Chemistry, Kyushu University, Hakozaki 6-10-1 Higashi-ku, Fukuoka 812-8581, Japan
[3]Adelaide Microscopy, University of Adelaide, 5005 South Australia, Australia
[4]CODES, University of Tasmania, Private Bag 126, Hobart, Tasmania 7001, Australia

ABSTRACT

Pyrite, the most abundant sulfide on Earth and a common component of gold deposits, can be a significant host for refractory gold. This is the first documentation of pore-attached, composite Au-telluride nanoparticles in "arsenic-free" pyrite. Trace elements mapping in pyrite from an intrusion-hosted Au deposit with orogenic overprint (Dongping, China) shows trails of tellurides overlapping Co-Ni-zonation. Intragranular microfracturing, anomalous anisotropy, and high porosity are all features consistent with devolatilization attributable to the orogenic event. The pyrite-hosted nanoparticles are likely the "frozen," solid expression of Te-rich, Au-Ag-Pb-bearing vapors discharged at this stage. Nanoparticle formation, as presented here, provides the "smallest-scale" tool to fingerprint Au-trapping during crustal metamorphism

Keywords: Arsenic-free pyrite, nanoparticles, Au-(Ag)-tellurides, devolatilization

INTRODUCTION

The properties of noble metal nanoparticles (NPs; <100 nm) and fine particles (100–2500 nm) in ores have important applications to mineral exploration, ore processing and environmental mitigation of coexisting toxic elements. The billion-dollar economic implications of "invisible gold" (Cook and Chryssoulis 1990) in pyrite for Au exploitation have driven substantial research aimed at characterizing, quantifying, and understanding how and why invisible gold, either as lattice bound or as NPs, occurs (Palenik et al. 2004; Reich et al. 2005; Large et al. 2009; Deditius et al. 2011). Arsenic-bearing pyrite illustrates the only known scenario for AuNP nucleation, whereby their formation is controlled by concentration above the As-saturation with Au/As molar ratio of ~0.02 (Reich et al. 2005). In As-bearing pyrite, Au and As are scavenged from low-temperature fluids typical of Carlin- and epithermal-type, from where AuNPs have been hitherto reported (Palenik et al. 2004; Deditius et al. 2011). In Carlin-type deposits, trapping of lattice-bound Au in As-bearing pyrite is dominant (Reich et al. 2005). Here we consider trapping of Au within pyrite in the absence of substitutional As by formation of telluride NPs during interaction with high-volatile fluids.

In many deposits, particularly those with protracted geological histories, Au often has a more diverse mineralogy, including Au-bearing tellurides (Cook et al. 2009a and references therein). There is a marked geochemical correlation between Au and chalcophile elements (Bi, Ag, Pb, Cu, etc.) with affinity to Te (CEs), forming telluride associations. In vent chimneys from the Silurian Yaman-Kasy volcanic-hosted deposit (Maslennikov et al. 2009), the presence of micro-inclusions was inferred in zones of As-free collomorph pyrite based on trace element correlations, suggesting they may have exsolved from pyrite Although not commonly reported, incorporation of CEs in pyrite is possible, as seen from the stunning oscillatory and sectorial zonation patterns for As, Cu, Ag, Te, and Se in pyrite from the high-sulfidation epithermal Au–Ag–Cu Pascua deposit (El Indio belt, Chile; Chouinard et al. 2005) or in orogenic and Carlin-type arsenian pyrite (Large et al. 2009).

BACKGROUND AND RATIONALE

Dongping, located on the margin of the North China Craton, is an example of a Au deposit with a telluride mineral signature. The mineralization, hosted by syenite intrusions, is attributed to either Paleozoic alkaline magmatism (Nie 1998) or to a Mesozoic magmatic-deformational event (Yanshanian orogeny) (Mao et al. 2003). The strong correlation between various types of textures in pyrite (brecciation, recrystallization, and porosity development) and Au concentration is consistent with multiple overlapping events (Cook et al. 2009b). Pyrite is a component of the Au-veins and host-rock alteration and is characterized by the presence of Au-, Au-(Ag)-, and Pb-telluride inclusions with spatial distributions that range from scattered to dense. Areas of clustered, micrometer-scale telluride inclusions were suggested to result from coupled-dissolution-reprecipitation-reactions (CDRR) between pre-existing pyrite and superimposed fluid(s) and the presence of NPs was postulated in such areas (Cook et al. 2009b). Ciobanu et al. (2011) showed micrometer- to submicrometer-scale details of such areas further supporting this interpretation. Cross-section high-resolution dual focused ion beam (FIB)–scanning electron microscopy (SEM) has shown that porosity is ubiquitously present within the areas of clustered telluride inclusions in pyrite. These inclusions, ranging in size from a few micrometers to hundred(s) of nanometers,

* E-mail: Cristiana.Ciobanu@adelaide.edu.au

0003-004X/12/0809–1515$05.00/DOI: http://dx.doi.org/10.2138/am.2012.4207

are multi-component, comprising a consistent association of Au-Ag-tellurides, altaite (PbTe) and gold. Moreover, an oriented porosity fabric is observed in pyrite hosting the fine particles. Documentation of NPs and their characteristics (size, composition, relationship to host pyrite) however requires an increase in image resolution of at least three orders of magnitude relative to the published data (Cook et al. 2009b; Ciobanu et al. 2011); this is the aim of the present work.

Methodology and results

Grain-scale element mapping was undertaken using laser ablation-inductively coupled plasma-mass spectroscopy (LA-ICP-MS; Deposit Item 1[1]) to see if pyrite from the area of clustered inclusions with maximum concentration of Au and CEs (Figs. 3c and 9 in Cook et al. 2009b) contains other traceable geochemical patterns. Here, the telluride inclusions are concentrated in zones of highest infiltration into the pyrite fed by the fractures, with the coarsest gold and galena inclusions observed in the fractures themselves. Element maps (Deposit Item 2[1]) reveal an underlying oscillatory zoning of Co and Ni throughout the area but slightly displaced by the fractures. No detectable As is present. FIB-SEM images and the foil shown in Figures 8b–8f of Ciobanu et al. (2011) derive from this area.

To find the presumed NPs within pyrite, the FIB-SEM technique (Ciobanu et al. 2011; Deposit Item 1[1]) was used to prepare site-specific foils for transmission electron microscopy (TEM). Although more than 20 FIB-cuts were made, only a minority of these could be thinned, and from those, only a few were suitable for imaging by TEM techniques (Deposit Item 1[1]). Pyrite grains from areas of clustered inclusions, as well as areas without clustered inclusions but with micrometer-sized fractures present, were sliced (Deposit Item 3[1]).

NPs were identified using high-angle annular dark-field–scanning transmission electron microscopy (HAADF-STEM) (Utsunomiya and Ewing 2003) from both textural contexts above but were most abundant in the first case. Similarly, NPs were also found in foils prepared by conventional ion milling of pyrite from the mapped area. The foil with the most NPs (Figs. 1–3, Deposit Items 4A–4C and 5[1]) was obtained by lifting and thinning the slice imaged in Figure 8a from Ciobanu et al. (2011). This is evidence that fields of NPs are present surrounding the larger inclusions, i.e., within the 2 µm thickness of the extracted slice, but are only fortuitously "captured" during the thinning process. The planes bearing NPs are, however, not necessarily identical with those hosting the larger inclusions.

The NPs are characteristically associated with microfractures and nanoscale porosity in pyrite (Fig. 1a). Electron diffraction patterns (EDPs) show that pyrite has the same orientation throughout the nanoparticle field (e.g., Fig. 1a, inset) and broadly across the entire foil. Importantly, the EDPs indicate the presence of an anisotropic pyrite (Bayliss 1977).

STEM-EDX compositional mapping of areas from this foil (Fig. 1b and Deposit Items 4B–4D and 5[1]) shows that the NPs all contain Te, but have different compositions, corresponding to petzite ($AuAg_3Te_2$), calaverite ($AuTe_2$), sylvanite and/or krennerite [$(Au,Ag)Te_2$], hessite (Ag_2Te), altaite, and intergrowths thereof. Although some 60 EDX point analyses were taken (Figs. 1c, 2b, and Deposit Item 4C[1]), only rarely do the analyses correspond to ideal telluride stoichiometry, suggesting that, in most cases, nanoscale mixtures of different tellurides are present. Simple Au-Ag inclusions were also identified (e.g., Deposit Item 4B[1]), showing that Au and Ag occur not only as tellurides but also as alloy, as in the larger inclusions (Cook et al. 2009b; Ciobanu et al. 2011).

Porosity is intrinsic to all NPs even if it is not always recorded on the 2D images. Identification of nanopores within the NPs is confirmed by the displayed inverse contrast on the HAADF-STEM (dark) and HR-TEM (bright) images of the same NP (Figs. 2a and 2c). Similar to the larger inclusions, proportions between pore and particle vary widely and the morphology changes from globular to quasi-geometric (Figs. 2d–2f). The size of the combined pore and associated NP ranges between 25 to ~100 nm, even though the NPs themselves attached to the larger pores may be only a few nanometers in diameter. Figures 3a–3d shows an agglomeration of composite NPs attached to a large pore (>100 nm) rather than a single NP. As identified from the EDX spectra, similar Au-Ag-telluride species, including petzite and sylvanite, were identified based on the fast Fourier transform of the HR-TEM images (Figs. 3e and 3f).

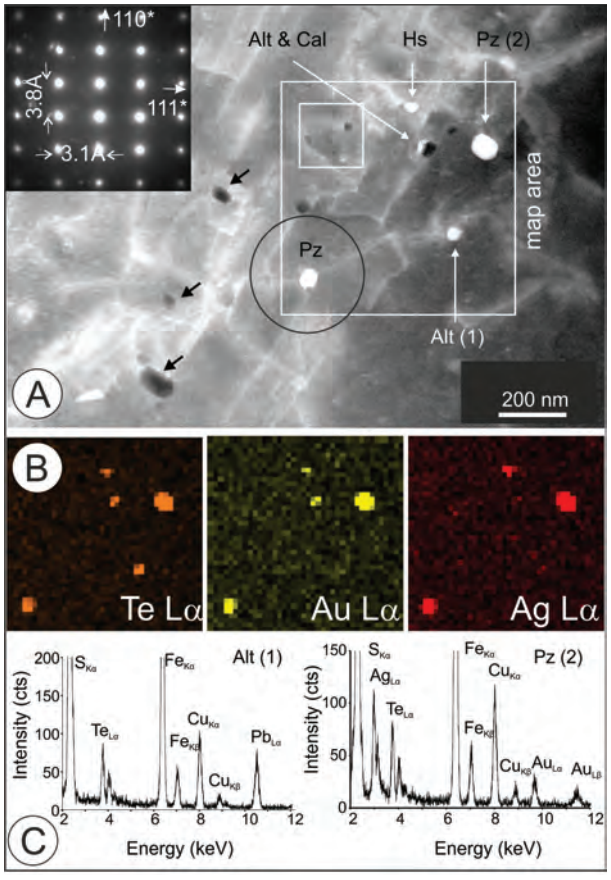

Figure 1. (**a**) HAADF-STEM image showing intragranular microfracturing, porosity, and pore-attached NPs in pyrite. Abbreviations: Alt, altaite; Au, native gold; Cal, calaverite; Hs, hessite; Pz, petzite. Inset is selected area of electron diffraction obtained from circled area showing zone [$\bar{1}\,\bar{1}2$] in pyrite, indexed using space group $P1$ ($a = b = c =$ 5.4166 Å) for anisotropic pyrite (Bayliss 1977). Black arrows: nanopores. (**b**) TEM-EDX element maps of the field of NPs in (large square in **a**) and located on Deposit Item 3A[1]. (**b**) TEM-EDX spectra of altaite and petzite in mapped area.

Discussion

The present study is the first case of Au-bearing NPs attached to pores in "As-free" pyrite formed under crustal conditions. The common pyrite orientation throughout the fields of NPs and the anomalous anisotropy (inferred from the lattice-type of pyrite, inset in Fig. 1a; Bayliss 1977) are both evidence that the observed textural pattern embedding the NPs corresponds to intragranular microfracturing rather than grain boundaries (Fig. 1a). Such features hint at a strain-induced deformation superimposed onto precursor pyrite in which a primary Co-Ni-zonation is preserved. These characteristics can be associated with crack healing following hydraulic brecciation via devolatilization, resulting in closure of short-lived porosity within a single crystal (Brantley et al. 1990). In the present study it is shown that this process allows for preservation of pore-attached NPs within single grains of highly strained pyrite. There is evidence from fluid inclusions

[1] Deposit item AM-12-080, Deposit items 1–5. Deposit items are available two ways: For a paper copy contact the Business Office of the Mineralogical Society of America (see inside front cover of recent issue) for price information. For an electronic copy visit the MSA web site at http://www.minsocam.org, go to the *American Mineralogist* Contents, find the table of contents for the specific volume/issue wanted, and then click on the deposit link there.

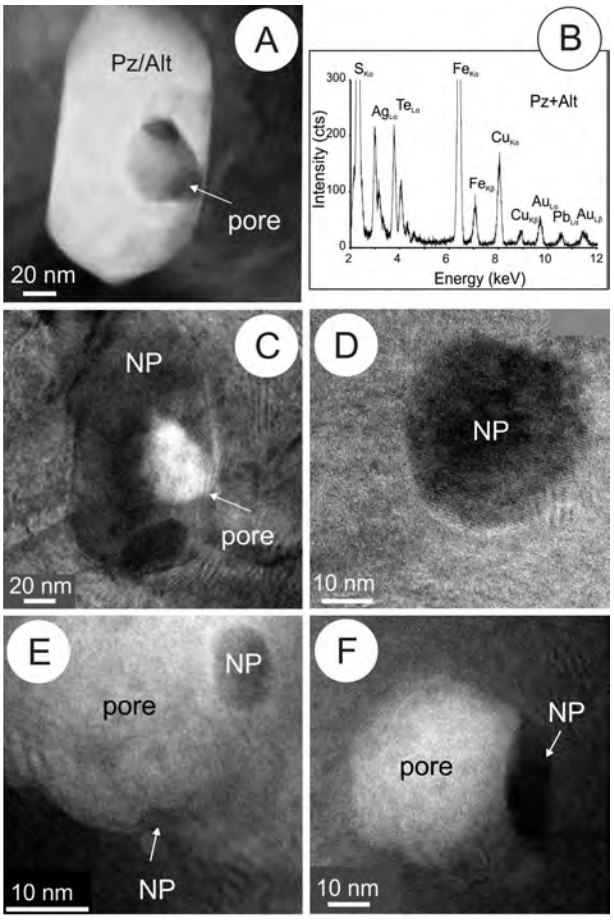

FIGURE 2. (**a**) HAADF-STEM image, (**b**) TEM-EDX spectrum, and (**c**–**f**) bright-field (BF) HR-TEM images of NPs showing their morphologies. Images **a** and **c** show the same NP and attached nanopore highlighting the inverse contrast on the two types of images.

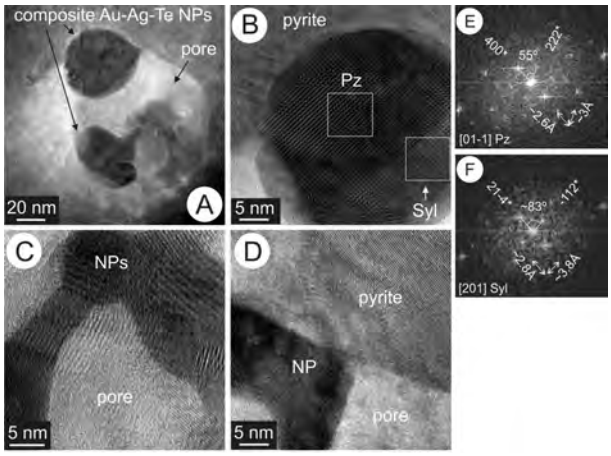

FIGURE 3. (**a**–**d**) Bright-field HR-TEM images of a large pore with attached NPs. Image (**b**) is a detail of the "upper" NP, showing the two-phase character. (**c**) Detail showing agglomeration of NPs. (**d**) Detail of the sharp contact between pyrite, NP, and pore. (**e**,**f**) Fast Fourier transform of the HR-TEM images as marked on **b**, showing zones [01$\bar{1}$] in petzite and [201] in sylvanite, respectively.

for a devolatilization event in a CO_2-H_2O-rich fluid at Dongping (Mao et al. 2003; as much as 60 mol% non-aqueous volatiles, mostly CO_2). Although metamorphic devolatilization (i.e., supporting an orogenic Au model for Dongping) cannot be entirely reconciled with the mantle He component of these fluids, Mao et al. (2003) favor a metamorphic origin. Pyrite formation is however attributable to an early stage (either Paleozoic or Mesozoic but predating the main orogenic Au stage) giving the range of overprinting textures reported here or in Cook et al. (2009b).

A tentative scenario for NP formation during devolatilization starts with hydraulic fracturing of pyrite. Fluids carrying Te-rich vapors and associated CEs wet microfractures and inflow into pores. This is feasible because Te is interpreted to be transported as a vapor species in hydrothermal fluids (McPhail 1995). The composite character of the NPs suggests that, at the time of Te discharge, other observed CEs, including Au, were co-partitioned from the fluid. Coalescence of Te-rich vapors from gas bubbles that may include other volatile components at locations of lowest tension to form solid (NP) phases. NP generation requires a high supersaturation at the time of discharge to induce a high nucleation density (Swihart 2003). Rapid crack healing, removing the source of supersaturation, results in isolation of pores and formation of closed systems and the rate of coalescence relative to particle-particle collision must have been sufficiently fast to prevent significant agglomeration (Ehrman et al. 1999), as observed here. Full crystallization of NPs occurs after crack sealing. The globular morphology is attributable to coalescence of vapors in the presence of a trapped (aqueous) liquid that filled the bulk of the bubble, whereas NPs with small pore volume preserved in the solid result from volume decrease during crystallization. The compositional similarity between larger inclusions and the NPs suggests that the initial Te- and CE-rich vapors were produced via an immiscibility event allowing for development of eutectic assemblages during cooling from ~400 °C comparable to those discussed for the larger inclusions (Cook et al. 2009b).

Fluid-rock interaction via CDRR is one potential enrichment mechanism whereby trace amounts of Au or other elements are extracted either from the host mineral or introduced from the infiltrating fluid. Replacement by CDRR results in a mineral precipitate that, even if the same as the parent mineral, will differ in trace element concentrations, porosity, inclusions, and/or grain size. The high transient-porosity associated with dissolution-reprecipitation (Putnis 2002) could also promote precipitation of these elements at the site of reaction. Cook et al. (2009b) showed that at Dongping, the CEs are found within telluride inclusions either relating to fracturing or concentrated in areas of clustered inclusions. Measured Au, Te, Ag, Bi, Pb, and Cu concentrations outside the clustered telluride inclusions in pyrite are variable (Cook et al. 2009b), but still much lower than in areas featuring fractures, shears and clustered inclusions; arsenic is, at maximum, only a few parts per million. This implies that Au and CEs could have been remobilized from the precursor pyrite but were more likely introduced by the infiltrating fluids. The fact that the NPs themselves include nanopores infers that their formation cannot be conciliated with a simple trace element exsolution from host pyrite.

Whether the devolalitization event attracted NP precipitation outside the pyrite or if this was restricted to specific interaction

between fluids and pyrite because some of the CEs were supplied by that pyrite cannot currently be constrained. It is more likely NPs were preserved in the latter where is evidence for more restricted fluid flow and rapid healing of intragranular microfractures.

The presence of NPs within areas of clustered inclusions (CDRR areas), and their similar characteristics in terms of composition and pore-association, indicates that both NPs and larger inclusions are attributable to the same devolatilization event. Porosity may be trapped during textural equilibration and results in trails of fluid inclusions (Putnis et al. 2005)—in the pyrite here, the analog of the fluid inclusions being the NPs. The presence of NPs outside areas of clustered inclusions but adjacent to fractures indicates that devolatilization affected areas of the pyrite beyond the clustered inclusions, the latter evolving via sustained infiltration fed by the fractures.

Similar to the pyrite discussed here, primary growth zones in zircon superimposed by complex secondary textures with abundant inclusions and redistribution of trace elements are interpreted in terms of chemical re-equilibration during interaction with fluids by CDRR (Geisler et al. 2007). Volume reduction and loss of material to the fluid acting as an agent for CDRR can result in zircon recrystallization in a low-strain environment (Rubatto et al. 2008). Alternatively, the microfracturing of pyrite prior to recrystallization in response to strain-induced deformation could have been associated with such volume reduction and porosity development. However, although some local recrystallization of pyrite might be assumed, it seems unlikely that the areas with clustered inclusions and NPs completely recrystallized, as this would not have allowed for preservation of the underlying Co-Ni zonation or have led to the observed anomalous anisotropy. Further work, including comparative study of pyrite outside areas of clustered inclusions is necessary to reach conclusions about the specific mechanisms of CDRR development from a devolatilization event affecting the pyrite itself.

Concluding remarks

The present study proves that abundant Au-bearing NPs exist and contribute to the total Au budget in "As-free" pyrite. The mineralogical speciation and distribution of such "invisible Au" has implications for improving recovery in deposits with a marked CE-rich signature.

The model presented here shifts the paradigm of trapping invisible Au in pyrite from As-mediated substitution and release of AuNPs upon supersaturation to the broader theme of fluid-mineral interaction under crustal conditions.

Analogous to fluid inclusions, pore-attached nanoparticles are likely the "frozen" expressions of a devolatilization event. When they occur in a common ore mineral, they provide a smallest-scale tool for tracking processes responsible for concentrating elements of economic interest.

Acknowledgments

We acknowledge the Australian Microscopy and Microanalysis Research Facility for access to the FEI Helios NanoLab at Adelaide Microscopy and staff of High-Voltage Electron Microscopy Laboratory, Kyushu University. S.U. acknowledges Science Grant no.20840035 of the Ministry of Education, Science and Culture. Leonid Danushevsky and Ian Little (CODES) are thanked for access and assistance with LA-ICP-MS mapping. We thank journal reviewers, Martin Reich, Ross Large, Valeriy Masselnikov, and an anonymous referee, as well as Rodney Ewing and Louis Cabri for their comments on an earlier version of the manuscript. This is TRaX contribution no. 230.

References cited

Bayliss, P. (1977) Crystal structure refinement of a weakly anisotropic pyrite. American Mineralogist, 62, 1168–1172.

Brantley, S.L., Evans, B., Hickman, S.H., and Crerar, D.A. (1990) Healing of microcracks in quartz: Implications for fluid flow. Geology, 18, 136–139.

Chouinard, A., Paquette, J., and Williams-Jones, A. (2005) Crystallographic controls on trace-element incorporation in auriferous pyrite from the Pascua epithermal high-sulfidation deposit, Chile-Argentina. Canadian Mineralogist, 43, 951–963.

Ciobanu, C.L., Cook, N.J., Utsunomiya, S., Pring, A., and Green, L. (2011) Focussed ion beam–transmission electron microscopy applications in ore mineralogy: Bridging micro- and nanoscale observations Ore Geology Reviews, 42, 6–32.

Cook, N.J., and Chryssoulis, S.L. (1990) Concentration of "invisible gold" in the common sulphides. Canadian Mineralogist, 28, 1–16.

Cook, N.J., Ciobanu, C.L., Spry, P.G., Voudouris, P., and the participants of IGCP-486 (2009a) Understanding gold-(silver)-telluride-(selenide) deposits. Episodes, 32, 249–263.

Cook, N.J., Ciobanu, C.L., and Mao, J. (2009b) Textural controls on gold distribution in As-free pyrite from the Dongping, Huangtuliang and Hougou gold deposits, North China Craton (Hebei Province, China). Chemical Geology, 264, 101–121.

Deditius, A.P., Utsunomiya, S., Reich, M., Kesler, S.E., Ewing, R.C., Hough, S.E., and Walshe, J. (2011) Trace metal nanoparticles in pyrite. Ore Geology Reviews, 42, 32–46.

Ehrman, S.H., Aquino-Class, M.I., and Zachariah, M.R. (1999) Effect of temperature and vapor-phase encapsulation on particle growth and morphology. Journal of Materials Research, 14, 1664–1671.

Geisler, T., Schaltegger, U., and Tomaschek, F. (2007) Re-equilibration of zircon in aqueous fluids and melts. Elements, 3, 43–50.

Large, R.R., Danyushevsky, L., Hollit, C., Maslennikov, V.V., Meffre, S., Gilbert, S., Bull, S., Scott, R., Emsbo, P., Thomas, H., Singh, B., and Foster, J. (2009) Gold and trace elements zonation in pyrite using Laser Imaging Technique: implications for the timing of gold in orogenic and Carlin-Style sediment-hosted deposits. Economic Geology, 104, 635–668.

Mao, J.W., Li, Y.Q., Goldfarb, R.J., He, Y., and Khin Zaw (2003) Fluid inclusion and noble gas studies of the Dongping gold deposit, Hebei Province, China: a mantle connection for mineralization? Economic Geology, 98, 517–534.

Maslennikov, V.V., Maslennikova, S.P., Large, R.R., and Danyushevsky, L.V. (2009) Study of trace element zonation in vent chimneys from Silurian Yaman-Kasy volcanic-hosted deposit (Southern Urals, Russia) using laser ablation–inductively coupled plasma mass spectrometry (LA-ICP-MS). Economic Geology, 104, 1111–1141.

McPhail, D.C. (1995) Thermodynamic properties of aqueous tellurium species between 25°C and. 350°C. Geochimica et Cosmochimica Acta, 59, 851–856.

Nie, F.J. (1998) Geology and origin of the Dongping alkali-type gold deposit, Northern Hebei Province, People's Republic of China. Resource Geology, 48, 139–158.

Palenik, C.S., Utsunomiya, S., Reich, M., Kesler, S.E., and Ewing, R.C. (2004) Invisible gold revealed: direct imaging of gold nanoparticles in a Carlin-type deposit. American Mineralogist, 89, 1359–1366.

Putnis, A. (2002) Mineral replacement reactions: from macroscopic observations to microscopic mechanisms. Mineralogical Magazine, 66, 689–708.

Putnis, C.V., Tsukamoto, K., and Nishimura, Y. (2005) Direct observations of pseudomorphism: compositional and textural evolution at a fluid-solid interface. American Mineralogist, 90, 1909–1912.

Reich, M., Kesler, S.E., Utsunomiya, S., Palenik, C.S., Chryssoulis, S.L., and Ewing, R.C. (2005) Solubility of gold in arsenian pyrite. Geochimica et Cosmochimica Acta, 69, 2781–2796.

Rubatto, D., Müntener, O., Barnhoorn, A., and Gregory, C. (2008) Dissolution-reprecipitation of zircon at low-temperaure, high-pressure conditions (Lanzo Massif, Italy). American Mineralogist, 93, 1519–1529.

Swihart, M.T. (2003) Vapor-phase synthesis of nanoparticles. Current Opinion Colloid Interface Science, 8, 127–133.

Utsunomiya, S., and Ewing, R.C. (2003) Application of high-angle annular dark field scanning transmission microscopy, scanning transmission electron microscopy-energy dispersive X-ray spectrometry, and energy-filtered transmission electron microscopy to the characterization of nanoparticles in the environment. Environmental Science & Technology, 37, 786–791.

Manuscript received April 25, 2012
Manuscript accepted June 11, 2012
Manuscript handled by Ian Swainson